Resonance Raman Analysis of the Mechanism of Energy Storage and Chromophore Distortion in the Primary Visual Photoproduct†

Elsa C. Y. Yan,‡,§ Ziad Ganim,‡,⊥ Manija A. Kazmi,§ Belinda S. W. Chang,|| Thomas P. Sakmar,§ and Richard A. Mathies*,‡

Department of Chemistry, University of California, Berkeley, California 94720, Howard Hughes Medical Institute, Rockefeller University, 1230 York Avenue, New York, New York 10021, and Department of Zoology, University of Toronto, 25 Harbord Street, Toronto, Ontario, Canada M5S 3G5

Received February 20, 2004; Revised Manuscript Received June 10, 2004

ABSTRACT: The vibrational structure of the chromophore in the primary photoproduct of vision, bathorhodopsin, is examined to determine the cause of the anomalously decoupled and intense C_{11}═C_{12} hydrogen-out-of-plane (HOOP) wagging modes and their relation to energy storage in the primary photoproduct. Low-temperature (77 K) resonance Raman spectra of Glu181 and Ser186 mutants of bovine rhodopsin reveal only mild mutagenic perturbations of the photoproduct spectrum suggesting that dipolar, electrostatic, or steric interactions with these residues do *not* cause the HOOP mode frequencies and intensities. Density functional theory calculations are performed to investigate the effect of geometric distortion on the HOOP coupling. The decoupled HOOP modes can be simulated by imposing ∼40° twists in the same direction about the C_{11}═C_{12} and C_{12}−C_{13} bonds. Sequence comparison and examination of the binding site suggests that these distortions are caused by three constraints consisting of an electrostatic anchor between the protonated Schiff base and the Glu113 counterion, as well as steric interactions of the 9- and 13-methyl groups with surrounding residues. This distortion stores light energy that is used to drive the subsequent protein conformational changes that activate rhodopsin.

Photoactive proteins play a vital role in a variety of light-energy and light-signaling processes that are characterized by pico- to femtosecond light-driven structural changes of a protein-bound chromophore followed by activated conformational changes of the protein. In systems such as rhodopsin (Rho)[1] (*1*), bacteriorhodopsin (*2*, *3*), halorhodopsin (*4*), photoactive yellow protein (*5*), and phytochrome (*6*, *7*), primary high-energy intermediates are produced with structurally perturbed chromophores. What is the nature of the protein−chromophore interactions that store the energy needed to drive subsequent protein conformational changes? To address this question, we have studied the photoactivation of rhodopsin, a dim-light photoreceptor, using a multidisciplinary approach that integrates Raman spectroscopy, mutagenesis, density functional theory (DFT) calculations, and bioinformatic analysis.

Rho is a paradigmatic G protein-coupled receptor, whose 7-transmembrane helical structure forms a binding pocket for 11-*cis*-retinal, which is covalently linked to Lys296 on helix 7. Within 200 fs after photoexcitation (*8*, *9*), the 11-*cis*-retinal protonated Schiff base (PSB) isomerizes to all-*trans*-retinal (ATR) with a quantum yield of 0.65 to form the primary photoproduct, Bathorhodopsin (*10*, *11*), which stores ∼30 kcal/mol or ∼60% of the incident photon energy (Figure 1) (*12*−*14*). Subsequently, the highly distorted chromophore relaxes, and the transduced energy is used to drive conformational changes in the opsin protein (*15*−*18*). Recently, we found that this structural evolution includes a retinal counterion switch from Glu113 in the dark state to Glu181 in the metarhodopsin I (Meta I) state (*19*). The Schiff base is then deprotonated upon Meta II formation, and Meta II couples with transducin to trigger the visual signal cascade (*20*, *21*).

Structural investigations on the primary photoproduct of rhodopsin have strived to determine how the photoisomerization of the 11-*cis*-retinal PSB chromophore is catalyzed and how the light energy is used to drive subsequent protein conformational changes. In 1974, Oseroff and Callender obtained the first Raman spectrum of Batho (*22*), revealing unique vibrational lines at ∼850, 875, and 920 cm^{-1} that are markers for the highly energetic and structurally distorted chromophore (Figure 1b). Proton transfer at the Schiff base and the formation of a tautomerized chromophore in the primary photoexcitation step were among the structures first proposed to explain the unique properties of Batho (*23*, *24*). Subsequent Raman experiments revealed a normal protonated

† Funding was provided by NIH Grant EY02051 (to R.A.M.). T.P.S. is an investigator of the Howard Hughes Medical Institute and an Ellison Foundation Senior Scholar.

* To whom correspondence should be addressed: Department of Chemistry, University of California, Berkeley, CA 94720. Phone: (510) 642-4192. Fax: (510) 642-3599. E-mail: rich@zinc.cchem.berkeley.edu.

‡ University of California.

§ Rockefeller University.

|| University of Toronto.

⊥ Current address: Department of Chemistry, Massachusetts Institute of Technology, Cambridge, MA 02139.

[1] Abbreviations: Rho, rhodopsin; Batho, bathorhodopsin; Meta I, metarhodopsin I; HOOP, hydrogen-out-of-plane; PSB, protonated Schiff base; E2, extracellular loop 2; H3, helix 3; DFT, density functional theory; DM, dodecyl maltoside; WT, wild type.

10.1021/bi0400148 CCC: $27.50
Published on Web 08/03/2004

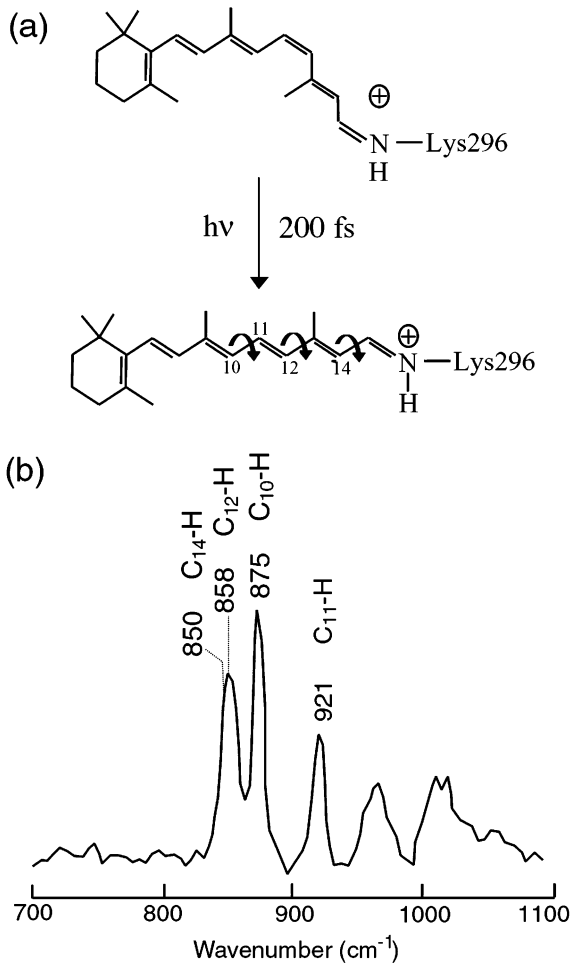

FIGURE 1: (a) Photon absorption triggers the 200 fs isomerization of the 11-*cis*-retinal chromophore in rhodopsin to form a highly energetic distorted structure in the primary photoproduct Batho. (b) Resonance Raman spectrum of Batho trapped at 77 K reveals strongly enhanced HOOP modes: $C_{10}H$ (875 cm^{-1}), $C_{11}H$ (921 cm^{-1}), $C_{12}H$ (858 cm^{-1}), and $C_{14}H$ (850 cm^{-1}). The intensities of these modes and the unusually low frequency of the C_{11}-HOOP mode at 921 cm^{-1} are the primary indicators for the perturbed structure about the C_{11}═C_{12} bond in this high-energy photoproduct (*28*).

Schiff base structure in Batho that disproved these ideas (*25*). Further measurements, exploiting isotopically labeled retinal derivatives from the Lugtenburg group, completed the assignment of the unique Batho lines to hydrogen-out-of-plane (HOOP) wagging modes of the chromophore (*26*−*28*).

Hydrogen-out-of-plane (HOOP) wags across a double bond generally couple strongly producing an in-phase mode at ~970 cm^{-1} and a lower wavenumber out-of-phase combination. However, the C_{11}═C_{12} HOOP modes of the Batho chromophore are unexpectedly decoupled producing a nearly isolated $C_{11}H$ wag at 920 cm^{-1} and $C_{12}H$ wag at 858 cm^{-1}. Since this assignment was achieved, the origin of this key structural observation about the structure of the Batho chromophore has remained unresolved despite a wide variety of theoretical models and experimental studies (*1*, *13*, *29*−*31*).

The recent crystal structure of bovine rhodopsin (*32*) prompted us to reexamine the origin of this HOOP mode perturbation. A surprising feature of the structure is that the β4 sheet of extracellular loop 2 (E2) aligns with the ethylenic

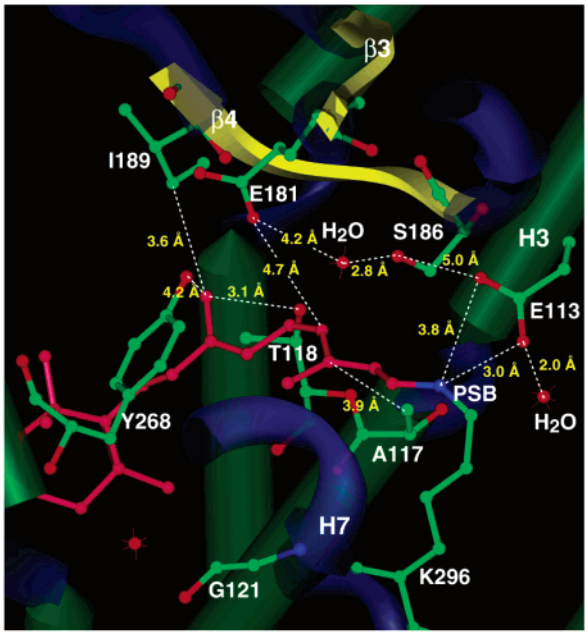

FIGURE 2: Retinal chromophore binding site from the crystal structure of bovine rhodopsin (*33*). Glu181 is situated just 4.7 Å away from C_{12} and may interact significantly with the chromophore. The strong electrostatic interaction of the PSB with its Glu113 counterion, as well as the hydrogen-bond chain connecting Glu113, Glu181, Ser186, and the retinylidene PSB via two water molecules, is also indicated.

chain of 11-*cis*-retinal, placing a potentially charged residue (Glu181) 4.7 Å from C_{12} as shown in Figure 2 (*32*−*35*). Through extensive biochemical and spectroscopic studies, we showed that Glu181 mutation produces a very modest perturbation of the absorption and Raman spectra of the Rho chromophore, and thus Glu181 must be protonated in the dark state (*19*, *36*). However, upon photolysis, the relative position of Glu181 and the chromophore is unknown so it is possible that Glu181 could significantly perturb the structure of the photoproduct chromophore.

Here, we have obtained low-temperature (77 K) resonance Raman spectra of Glu181 mutants of bovine rhodopsin to test the hypothesis that an electrostatic or a dipolar interaction between Glu181 and chromophore decouples the C_{11}═C_{12} HOOP modes in Batho. Surprisingly, the spectra of the Glu181 mutants exhibit only mild mutagenic alterations of the frequencies of the decoupled C_{11}═C_{12} HOOP modes in the Batho chromophore, indicating that direct electrostatic, dipolar, or steric interaction with Glu181 is not significant. Having eliminated this possibility, we then perform DFT calculations of the photoproduct vibrational structure to explore whether the previously identified (*27*) geometric distortion might be sufficient to explain the decoupled HOOP frequencies. A unique set of twists is identified that reproduces the characteristic decoupled vibrational frequencies of Batho. Furthermore, a comparison of Batho Raman spectra of a variety of native visual pigments and of bovine rhodopsin analogues viewed in the context of their protein sequences allows us to propose that steric interactions with the 9- and 13-methyl groups, as well as the electrostatic anchoring of the protonated Schiff base group are the origin of the structural constraints that cause the HOOP decoupling. Protein-mediated distortions of conjugated C═C bonds are thus implicated as a general mechanism for storing the light

energy that is used to drive subsequent conformational changes in light-activated proteins.

EXPERIMENTAL SECTION

Site-directed point mutations were prepared using the QuickChange method (Stratagene) and verified by sequencing. The mutant pigments were transiently expressed in COS cells, harvested, regenerated with 11-*cis*-retinal, and purified by an immunoaffinity adsorption procedure (*37*, *38*). Pigments were prepared in 100 mM NaCl and 0.1% dodecyl maltoside (DM) in 50 mM phosphate buffer at pH 6.8 and concentrated to ~1.5 OD at 500 nm. The pigment solutions were mixed with an equal volume of glycerol and then transferred to a 600 μm ID capillary that was cooled to ~77 K in a thermally insulated Harney−Miller cell by chilled nitrogen gas.

Resonance Raman spectra of pigments in the Batho state were obtained using a 496- or 488-nm probe beam from an argon ion laser (Spectra-Physics 2020) and a coaxial 568-nm pump beam from krypton ion laser (Spectra-Physics 2025). The pigment solutions were irradiated by a blue probe beam to obtain Raman spectra of a steady-state mixture of approximately 25% Rho, 15% isorhodopsin (Iso), and 60% Batho (*22*). The coaxial 568-nm pump beam was added at sufficient power to drive down the Batho concentration, facilitating the assignment of the Batho spectra (*39*). The scattering was dispersed by a double spectrograph (Spex 1400) and detected by a CCD (LN/CCD-1100/PB, Princeton Instruments). The spectra were calibrated against cyclohexane and cyclohexanone. The reported frequencies are accurate to 2 cm^{-1}, and the spectral resolution is 2 cm^{-1}.

DFT calculations were carried out using Gaussian 98 (*40*) with implementation of Becke's Three Parameter Hybrid Functional using the Lee, Yang, and Parr Correlation Functional (B3LYP) (*41*). This level of theory with the 6-31G(d) basis set has been used (*42*−*45*) to calculate normal-mode frequencies and Raman activities of 30−60-atom organic molecules. The initial geometry for 6-*s*-*cis* ATR was taken from the crystal structure (*46*). Dihedral angles about the C_{11}═C_{12} and/or C_{12}−C_{13} bonds were set as constants, while the remaining degrees of freedom were allowed to relax in the electronic structure optimization (*47*). These optimizations show that twists about the C_{11}═C_{12} and C_{12}−C_{13} bonds trigger deviations of the neighboring ethylenic chain from planarity. For example, setting the dihedral twists of the C_{11}═C_{12} and C_{12}−C_{13} bonds to −40° in the ATR−PSB model induces twists about the C_9═C_{10} (−6.0°), C_{10}−C_{11} (8.8°), C_{13}═C_{14} (−1.9°), and C_{14}−C_{15} (−1.9°) bonds upon structural optimization. The normal-mode frequencies were then calculated with the optimized constrained geometry using the same level of theory and basis set. A linear scaling factor of 0.9538 was determined by a least-squares fit of the 800−1050 cm^{-1} region of the calculated HOOP frequencies to the experimentally observed frequencies with the *y* intercept equal to 0 (*48*). The torsional constraints on the C_{11}═C_{12} and C_{12}−C_{13} bonds in the calculation project primarily onto displacements along the low-frequency (<550 cm^{-1}) dihedral torsions (*49*) that are energetically well-separated from the HOOP region (830−970 cm^{-1}); their effect on the HOOP modes is thus negligible.

The masses of the coupled hydrogens other than $C_{11}H$ and $C_{12}H$ were set to 10.0 amu to drop their corresponding wagging frequencies by ~300 cm^{-1}, thereby removing the interaction of the heavy HOOP wagging and rocking modes with the individual C_{11} and C_{12} HOOP modes. The resulting frequencies allow us to study the intrinsic effect of dihedral twists at C_{11}═C_{12} and C_{12}−C_{13} on the C_{11}═C_{12} HOOP, decoupling without interference from mixing and/or coupling with other vibrational modes (*28*). A mass of >2.0 was chosen because we found that the deuterated rocking modes dropped to the 900−960 cm^{-1} (*51*) region and complicated the interpretation of the calculated HOOP results. Once the intrinsic effect of torsional distortion on the HOOP modes was identified, key limiting calculations were repeated with normal hydrogen to verify the validity of our conclusions.

The calculations were repeated for the ATR−PSB to determine whether the twisting results are also pertinent for the PSB chromophore. The initial ATR−PSB structure was constructed by replacing the terminal oxygen of ATR with a $NHCH_2CH_3$ group using the anti C═N configuration. To mimic the electronic properties of the Glu113 counterion, a Cl atom was added initially in line with the N−H bond and allowed to minimize. The ion pair was maintained throughout the calculation, as determined by a Mulliken atomic charge analysis. The calculated normal modes were visualized in Molden (*50*).

RESULTS

The resonance Raman spectra of Rho and selected mutants (E181Q and S186A) at ~77 K are presented in Figure 3. In Figure 3a, irradiation of wild-type Rho with the 496-nm probe beam creates a steady-state mixture of Rho, Iso, and Batho. Two intense ethylenic bands at 1537 cm^{-1} for Batho and at 1550 cm^{-1} for the mixture of Rho and Iso are observed. The characteristic decoupled HOOP vibrational bands of Batho at 857, 875, and 920 cm^{-1} are also prominent. A coaxial 568-nm pump beam was then added to drive down the Batho concentration. The intensity of the Batho ethylenic band (1537 cm^{-1}) and the Batho HOOP bands (856, 874, and 920 cm^{-1}) decreases, confirming a depletion of Batho in the steady-state mixture. Subtracting the pump + probe spectrum from the probe-only spectrum to eliminate the 1550 cm^{-1} band yields the Batho spectra. When this experiment is performed on the E181Q mutant with a 496-nm probe beam and the Ser186 mutant with a 488-nm probe beam, the two ethylenic bands are not as distinct. However, the intense decoupled HOOP bands in the 850−950 cm^{-1} region are clearly observed. Addition of the 568-nm pump beam drives down the concentration of the Batho photoproduct allowing subtractions to yield the Batho spectra of the mutants. The observation of the steady-state mixture and of the characteristic HOOP modes of the primary photoproducts for the mutant pigments at low temperature (77 K) demonstrates that their primary photochemistry is very similar to that of the native pigment.

Figure 4 presents expanded views of the resonance Raman spectra of wild-type (WT) Batho and its E181D, -Q, and -F mutants. The Batho spectrum of the E181D mutant exhibits the same ethylenic stretching, C═N stretching, and HOOP wagging vibrational frequencies as the WT (±2 cm^{-1}), suggesting that the E181D mutagenic perturbation to the structure of the primary photoproduct is negligible. The Batho spectra of E181Q and E181F are more significantly

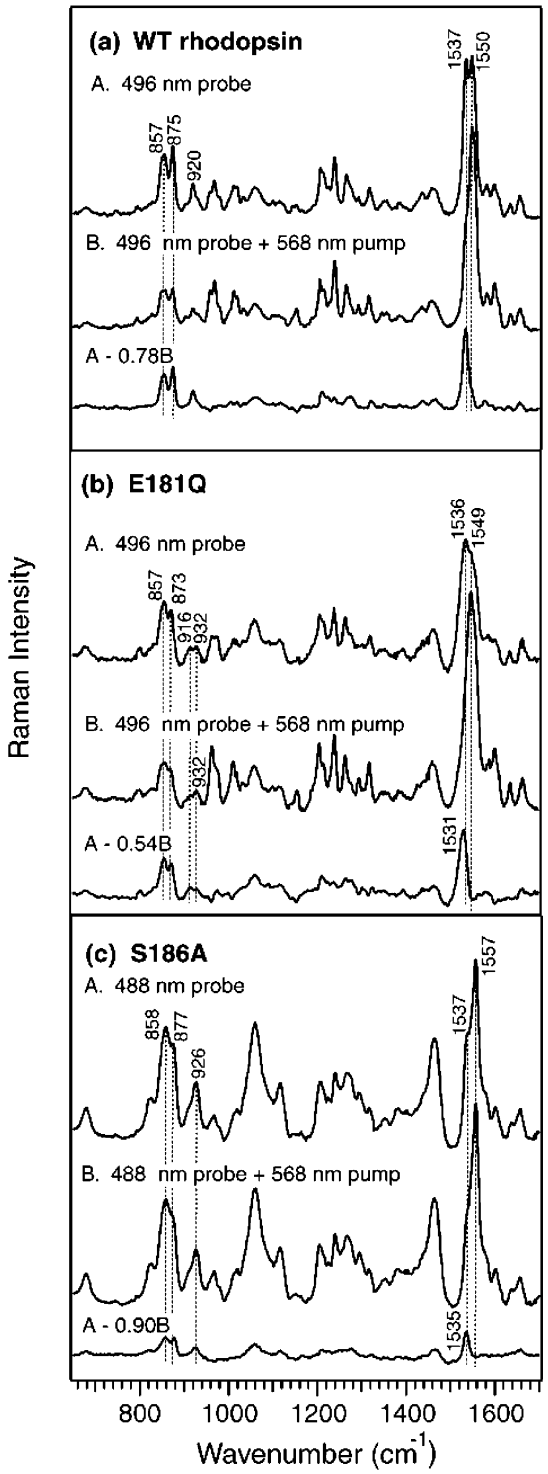

FIGURE 3: Resonance Raman spectra of low-temperature (77 K) photostationary steady-state mixtures of Rho, Batho, and Iso from (a) the WT pigment and (b) E181Q and (c) S186A mutants. The steady-state mixtures of the pigments at ~77 K are probed with 496 nm for the WT and E181Q and with 488 nm for S186A. The pigments are irradiated with a pump beam at 568 nm to drive down the Batho concentration shown in spectra B. Subtracting the pump + probe spectra from the probe-only spectra to eliminate the 1550-cm^{-1} line of the ethylenic stretching of Rho and Iso yields the Batho spectra.

altered. The C=N stretching shifts from 1657 to 1664 cm^{-1} for E181Q and to 1663 cm^{-1} for E181F, suggesting that the PSB group is in a stronger hydrogen-bonded environment in the mutant pigments (*52*, *53*). The C=C stretching frequency is shifted from 1536 to 1531 cm^{-1} for both E181Q and E181F, suggesting a red shift in their UV−vis absorption spectra. The mild perturbations of the mutant Batho spectra are consistent with a protonated (neutral) Glu181 in the Batho state in agreement with our previous conclusion that Glu181 is protonated in the dark state (*19*, *36*). Most importantly, all Glu181 mutant Batho spectra exhibit the characteristic 3 bands in the HOOP region (850−950 cm^{-1}) within 4 cm^{-1} of their native frequencies. The consistent frequency and intensity patterns of the HOOP modes suggest that the C_{11}=C_{12} HOOP wags in the mutants remain decoupled despite these mutations.

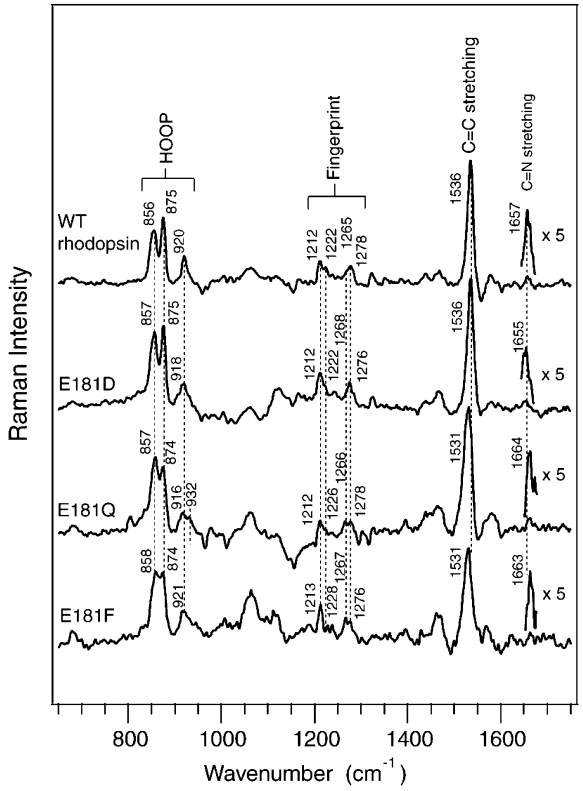

FIGURE 4: Comparison of resonance Raman spectra of WT Batho and its E181D, E181Q, and E181F mutants.

Figure 5 presents a spectral decomposition of the HOOP region of the Batho spectra of the Glu181 and Ser186 mutants compared with the WT pigment. The E181D and E181F spectra exhibit the same C_{11}-HOOP frequency (920 cm^{-1}) as the WT within the experimental error (2 cm^{-1}), while the S186A and S186I spectra exhibit an upshift of 4 cm^{-1}. The bandwidths of the ~920-cm^{-1} line for the mutants (20−23 cm^{-1}) are broader than that for the WT (13 cm^{-1}). We reproducibly found that two Gaussian peaks at 916 and 932 cm^{-1} are necessary to fit the C_{11}-HOOP band of E181Q. This suggests that there might be two different Batho chromophore structures for E181Q, though we cannot exclude the possibility that an incomplete subtraction of the Rho and Iso contribution leads to the observation of the 932-cm^{-1} line (see Figure 3). The C_{10}-HOOP vibrational frequency of the mutants is the same as that of the WT within the experimental error (2 cm^{-1}), showing that these mutations have essentially no effect on the chromophore structure near C_{10}. The third observable HOOP band at ~856 cm^{-1} is decomposed to two Gaussian peaks corresponding to the C_{14}-HOOP at ~850 cm^{-1} and C_{12}-HOOP at ~858 cm^{-1}. The decomposed C_{12}- and C_{14}-HOOP bands of the mutants are

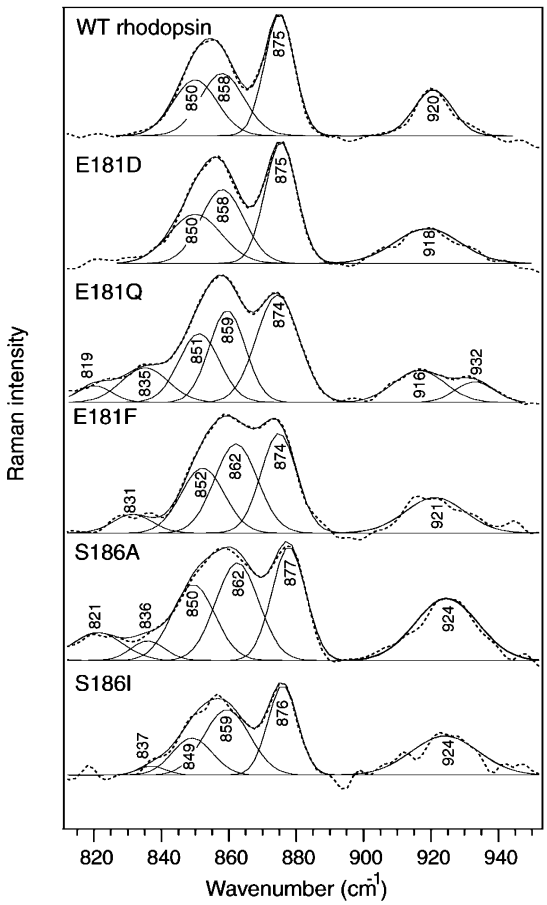

FIGURE 5: Spectral decomposition of the HOOP region of the resonance Raman spectra of WT Batho and its E181D, E181Q, E181F, S186A, and S186I mutants. The spectra of the Ser186 mutants were obtained in the same manner as the Glu181 mutants using a probe beam at 488 nm. Spectral decompositions were obtained by Gaussian fits to the bands.

within 4 cm^{-1} of the WT control. Lower wavenumber lines at ~820 and ~835 cm^{-1}, previously assigned as combinations of out-of-plane modes (*28*), are more pronounced in the E181Q, E181F, and S186A spectra. The intensity ratios of the ~856−875 cm^{-1} bands in these pigments are also higher, indicating a geometric perturbation to the ethylenic chain.

Vibrational Modeling. Because Glu181 and Ser186 mutations did not produce a significant alteration of the Batho HOOP modes and, on the basis of the crystal structure, there are no other obvious perturbing residues near the C_{11}=C_{12} bond (see Figure 2), we used DFT calculations to explore whether conformational and/or configurational distortion might be sufficient to produce the unique vibrational frequencies of the C_{11}- and C_{12}-HOOP modes in Batho. In the calculations, the dihedral twists about the C_{11}=C_{12} and/or C_{12}−C_{13} bonds were fixed and then the chromophore structure was optimized. Figure 6 presents a selection of the calculated intrinsic C_{11}-H and C_{12}-H wagging frequencies when various fixed twists are applied. We were looking for a perturbation that would produce a significant reduction of the intrinsic C_{12}H wagging frequency thereby producing a large splitting between the intrinsic C_{11}H and C_{12}H wagging modes. For the ATR calculation, simultaneous opposite sense twists as large as 40° (e.g., 40°, −40°) give insignificant lowering of the C_{12}H wag compared with the experimental

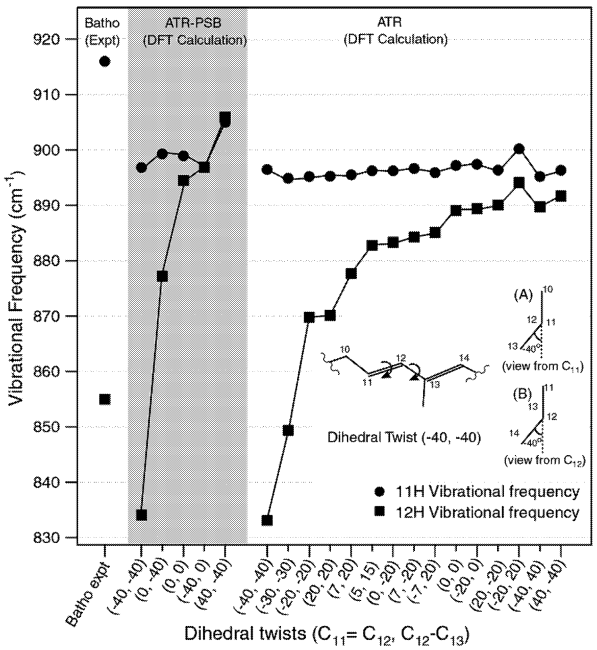

FIGURE 6: Calculated intrinsic C_{11}- and C_{12}-HOOP frequencies for ATR and the ATR−PSB (shaded region) as a function of the indicated fixed C_{11}=C_{12} and C_{12}−C_{13} dihedral angles. The experimental HOOP mode frequencies of Batho are shown at the left. (A) and (B) are projections of the chromophore geometry viewed from C_{11} and C_{12}, respectively, showing the −40° dihedral twists about the C_{11}=C_{12} and C_{12}−C_{13} bonds.

splitting of ~60 cm^{-1}. Twisting at just the C_{11}=C_{12} bond by up to 20° also induces an insignificant frequency lowering in the ATR calculations. The intrinsic C_{12}H wag frequency is more sensitive to twists about the C_{12}−C_{13} bond; a 20° dihedral twist lowers this mode by 13 cm^{-1} in ATR. Twisting in the same sense about *both* the C_{11}=C_{12} and C_{12}−C_{13} dihedral angles consistently dropped the C_{12}H wag by ~1.5 cm^{-1} per degree with a <10 cm^{-1} shift of the C_{11}H wag. The −40°/−40° calculation gives a C_{11}H=C_{12}H splitting of 63 cm^{-1}, yielding the closest match to the Batho experiment of the 15 calculated structures.

Similar results were obtained for the ATR−PSB calculations, which are presented in the shaded region of Figure 6. Twists about C_{11}=C_{12} and C_{12}−C_{13} in the opposite sense (40°, −40°) had no significant effect, and twisting just one bond by up to 40° produced a 20 cm^{-1} frequency reduction only when the C_{12}−C_{13} bond was distorted. The C_{11}H and C_{12}H wagging modes were more effectively decoupled by applying twists about both bonds simultaneously, and the −40°/−40° structure gives a 61 cm^{-1} splitting, which closely matches the experimental value of 63 cm^{-1} for Batho. The effect of dihedral twists at other positions was also explored extensively but none of them significantly alter the C_{11}=C_{12} HOOP modes.

Figure 7 presents the relative contributions of the C_{11}-H and C_{12}-H wags to different normal modes for the ATR−PSB chromophore using conventional hydrogen masses. For the planar (0, 0) molecule, the C_{11}- and C_{12}-HOOP wags are strongly and roughly equally coupled producing two in-phase modes at 960−970 cm^{-1}. Additional out-of-phase combinations are found from 825 to 850 cm^{-1} that are more dominated by C_{12}-H character consistent with the experiment (*28*, *48*). For the highly twisted (−40, −40) molecule, the pattern collapses to an isolated C_{11}-H wag at ~930 cm^{-1},

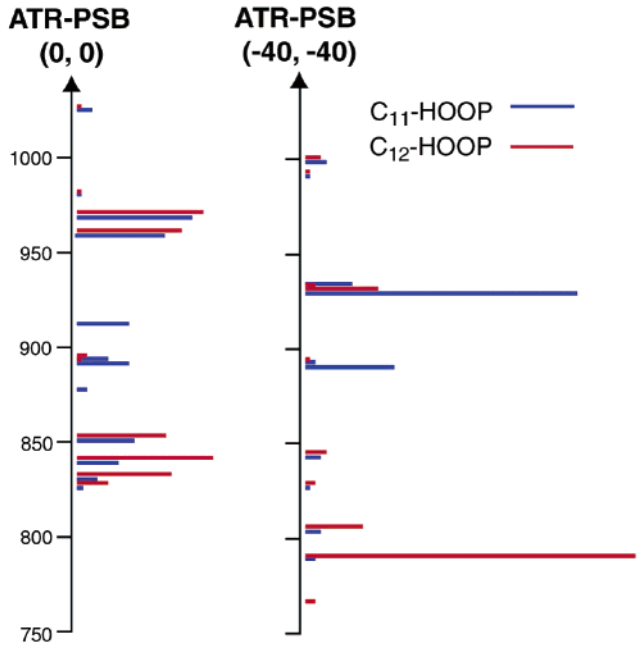

FIGURE 7: Relative contributions of C_{11}-H and C_{12}-H wagging motion to different normal modes for planar (0, 0) and twisted (−40, −40) ATR−PSB. C_{11}-H character is indicated in blue, and C_{12}-H character is indicated in red.

while the downshifted normal modes at ∼800 cm^{-1} are predominately C_{12}-H wagging. This result reproduces the experimentally observed decoupling of the C_{11}-H and C_{12}-H wags in Batho and the anomalously low C_{12}-H wag frequency analyzed by Palings et al. (*28*). This result illustrates two important points. First, the modes for the undistorted or slightly distorted molecule are sufficiently mixed and coupled that it would be hard to systematically explore the effect of conformational distortion without the use of heavy hydrogen as done here. Second, the pattern identified in these calculations is a robust effect, which is clearly in evidence in the (−40, −40) calculation for the molecule with conventional hydrogen masses. The intrinsic frequencies identified in our calculations consequently provide clear and quantitative indicators to explore the effect of torsional distortion on the HOOP frequencies and couplings.

DISCUSSION

To identify the cause of the decoupling of the C_{11}═C_{12} HOOP modes in the primary photoproduct of vision, we first hypothesized that Glu181 and Ser186, being dipolar residues that are near to the center of the chromophore, might perturb the photoproduct and cause the characteristic anomalous HOOP frequencies. The Batho Raman spectra of Glu181 and Ser186 mutants clearly demonstrate only mild mutagenic perturbation to the vibrational structure, indicating that direct dielectric, charge, or steric interaction with the polar residues Glu181 or Ser186 does not cause the decoupling of the C_{11}═C_{12} HOOP modes.

We then explored whether the decoupling of the C_{11}═C_{12} HOOP modes could be achieved by pure geometric distortion. Although NMR studies by Smith's group (*29*, *30*) as well as theoretical studies (*13*, *31*) have suggested that geometric distortion of the chromophore is important in the energy-storage mechanism, no detailed geometry and specific chromophore−protein interactions have been put forward to account for the HOOP frequencies. The highly unique and unusual vibrational structure of Batho has thus remained an enigma since its first observation in 1974 (*22*). To address this challenge, we calculated the Raman vibrational frequencies of the C_{11}- and C_{12}-HOOP modes with a wide variety of distortions from planarity. The experimentally observed C_{11}═C_{12} decoupling is successfully simulated only when dihedral twists of ∼40° were imposed about the C_{11}═C_{12} and C_{12}−C_{13} bonds in the same sense for both ATR and ATR−PSB. Our calculations further indicate that the terminal group does not mechanistically change the nature of the distortions that cause the C_{11}═C_{12} decoupling. The calculated ATR and ATR−PSB structures have a torsional energy of 14.1 and 15.6 kcal/mol, respectively, compared to a total of ∼30 kcal/mol in Batho (*12*, *14*). This calculated energy is only a qualitative estimate because all of the protein interactions have not been included, but this result does indicate that torsional distortions are an important energy-storage component. The absolute sense of the twisting cannot be determined by our calculations alone because the (+, +) and (−, −) twists are equivalent in the calculation. The twists about the C_{11}═C_{12} and C_{12}−C_{13} bonds in Batho propagate along the ethylenic chain causing the neighboring bonds to be distorted from planarity as well. The resulting out-of-plane displacement at the C_9═C_{10}, C_{10}−C_{11}, C_{13}═C_{14}, and C_{14}−C_{15} bonds is anticipated to be the origin of the HOOP intensities at C_{10}H and C_{14}H (*28*).

Protein-Mediated Distortion. Because distortion along the ethylenic chain is sufficient to cause the C_{11}═C_{12} HOOP decoupling in the Batho chromophore, it is pertinent to examine the crystal structure to consider the molecular origin of this distortion. A comparison of the Batho Raman spectra and the protein sequences of a variety of visual pigments provides insight into the origin of the distortion. Figure 8 compares the positions of the HOOP bands in the Batho spectra of a variety of visual pigments. All vertebrate rod pigments including bovine rhodopsin, toad red rod, anglefish rod, gecko blue rod, and bullfrog green rod (*54*) give a typical Batho HOOP pattern. The Batho HOOP frequencies of the red cone pigment, chicken iodopsin (*55*), deviate from the standard HOOP frequencies probably because of the more delocalized electronic structure needed to achieve red absorption, but the pattern of three HOOP bands is preserved. The Glu181 and Ser186 mutations do not perturb the HOOP modes, whereas the Glu113 mutations change the HOOP pattern from three bands to two at ∼888 and 934 cm^{-1} (*53*). Invertebrate octopus rhodopsin (*56*), which does not have a glutamic acid at the position corresponding to 113, gives the same phenotype as Glu113 mutants. This suggests that the electrostatic attraction or anchoring between the PSB group and Glu113 is an important factor in determining the HOOP frequencies and intensities in Batho. The Batho spectra of bovine rhodopsin regenerated with 9- and 13-demethyl retinal analogues also exhibit an altered HOOP pattern (*26*), but the spectrum of the pigment regenerated with 5-demethyl retinal (Eyring and Mathies, unpublished results) exhibits normal Batho HOOP modes. This indicates that the steric interactions of the 9- and 13-methyl groups with the opsin protein also play a role in determining the HOOP decoupling in Batho.

Protein sequence alignments in the counterion and E2 regions reveal the residues that are required for twisting the

Table 1: Rhodopsin Residues in the E2 Loop, Counterion, 9-Methyl, and 13-Methyl Regions[a]

	H3			E2																		H5	H6	H7		
	counterion			β3					β4																	
	113	117	**118**	177	178	179	180	181	182	183	184	185	186	187	**188**	**189**	190	**191**	192	195	**207**	265	292	295	296
bovine	E	A	**T**	R	Y	I	P	E	G	M	Q	C	S	C	**G**	**I**	D	**Y**	Y	H	**M**	W	A	A	K
toad P502	E	A	**T**	R	Y	I	P	E	G	M	Q	C	S	C	**G**	**V**	D	**Y**	Y	K	**M**	W	A	A	K
cichlid P500	E	A	**T**	R	Y	I	P	E	G	M	Q	C	S	C	**G**	**V**	D	**Y**	Y	A	**M**	W	A	A	K
gecko P467	E	A	**T**	R	F	I	P	E	G	M	Q	C	S	C	**G**	**P**	D	**Y**	Y	N	**M**	W	A	A	K
bullfrog P430	E	A	**T**	R	Y	I	P	E	G	L	Q	C	S	C	**G**	**P**	D	**W**	Y	N	**I**	W	S	A	K
chicken P571	E	V	**S**	R	Y	W	P	H	G	L	K	T	S	C	**G**	**P**	D	**V**	F	S	**L**	W	A	A	K
octopus P427	Y	G	**G**	A	Y	V	P	E	G	I	L	T	S	C	**S**	**F**	D	**Y**	L	D	**M**	W	V	A	K

[a] Residues < 5 Å from the 9-methyl group are bold, and residues < 5 Å from the 13-methyl group are italicized. H3, -5, -6, and -7 are rhodopsin helices. β3 and β4 are β sheets on E2.

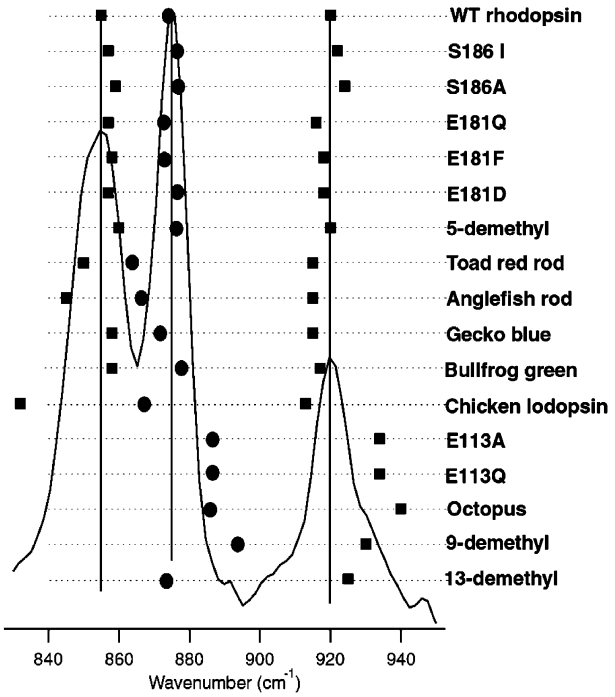

FIGURE 8: Summary of the HOOP bands of the primary photoproducts in resonance Raman spectra of different visual pigments. The peak positions of HOOP modes in the Batho state are indicated for the WT bovine rhodopsin, S186I, S186A, E181D, E181Q, E113A, E113Q (*53*), 5-demethyl rhodopsin, 9-demethyl rhodopsin (*26*), octopus rhodopsin (*56*), toad (*Bufo marinus*) red rod, angelfish (*Pterophyllum scalare*) rods, gecko (*Gekko gecko*) rod, bullfrog (*Rana catesbeiana*) rod (*54*), and chicken (*Gallus domesticus*) iodopsin (*55*).

ethylenic chain resulting in the observed HOOP decoupling. In Table 1, five residues marked in bold face (118, 188, 189, 191, and 207) are within 5 Å of the 9-methyl group and five underlined residues (117, 265, 292, 295, and 296) are within 5 Å of the 13-methyl group (Figure 2). Among these 10 residues, octopus rhodopsin inherits amino acids at positions 117, 118, 188, and 189 that are different from the rest of the visual pigments. For example, while all pigments have Gly at position 188, octopus has a Ser. The replacements in octopus rhodopsin are hence A117G, T118G, G188S, and P189F. Considering that the 9- and 13-methyl groups are required to observe the Batho HOOP modes, we suggest that steric interaction of the 13-methyl group with Ala117 and of the 9-methyl group with Thr118, Gly188, and Ile189 are crucial for the distortion of the Batho chromophore. Consistently, low-temperature FTIR experiments showed that the hydroxyl group at Thr118 undergoes structural changes in the Rho−Batho transition (*57*). Figure 8 reveals that the electrostatic anchor between the PSB group and the Glu113 counterion works together with the steric interactions at the 9- and 13-methyl groups to provide three constraints that mediate the distortion of the ethylenic chain. When any one of these constraints is released, the twisting of the chromophore is altered as reflected by the modified HOOP mode patterns.

To determine the absolute conformation and orientation of the Batho chromophore in the binding pocket, we need to define the direction of rotation about the C_{11}=C_{12} and C_{12}−C_{13} bonds in the photoisomerization. The initial conformation is determined by steric constraints on the 11-*cis* chromophore in the binding pocket, which are revealed in the crystal structure (*32*−*34*). The C_{12} is only 3.3 Å from the backbone oxygen of Cys187 (*58*), and the 13-methyl group is only 3.4 Å from the C_{10}H group. Interestingly, steric repulsion between the 13-methyl group and C_{10}H pushes the methyl group out of the ethylenic plane and closer to the E2 loop as shown in Figure 9A (*33*). To specify the absolute conformation, we use the conventional definition of the dihedral angle (*59*, *60*). As revealed from the crystal structure, the dihedral angle about the C_{12}−C_{13} bond is 150°, so the 13-methyl group is 0.8 Å above the C_{11}=C_{12}−C_{13} plane; the dihedral angle about C_{10}−C_{11} is 163°, so the C_{10}H is 0.4 Å below the C_{10}−C_{11}=C_{12} plane (see Figure 9A). To release the steric repulsions of C_{12} from Cys187 and of the 13-methyl group from C_{10}H, the isomerization at C_{11}=C_{12} occurs such that it rotates in a clockwise sense (viewed from lysine 296) to push the C_{12}H down away from E2 and to bring the 13-methyl group up away from C_{10}H. A rotation of the C_{11}=C_{12} bond through 140° with a compensating reverse rotation about the C_{12}−C_{13} bond through ~40° will lead to the absolute dihedral angle conformation of −140° at both the C_{11}=C_{12} and C_{12}−C_{13} bonds (Figure 9B), which is equivalent to the (−40, −40) twist presented in Figure 6. Compensating distortion of the adjacent single bond, following double-bond photoisomerization, was also suggested to be an important mechanism for energy storage in the primary photoevents of bacteriorhodopsin (*61*) and photoactive yellow protein (*62*).

The four important residues at positions 117, 118, 188, and 189 that produce the steric barriers for the methyl groups are located exclusively on E2 and H3. This observation is consistent with our recently proposed model, suggesting that the movement of E2 and H3 coordinated by the Cys110−Cys187 disulfide bond is crucial in the photoactivation process (*19*). In recent Raman studies, Pan et al. demon-

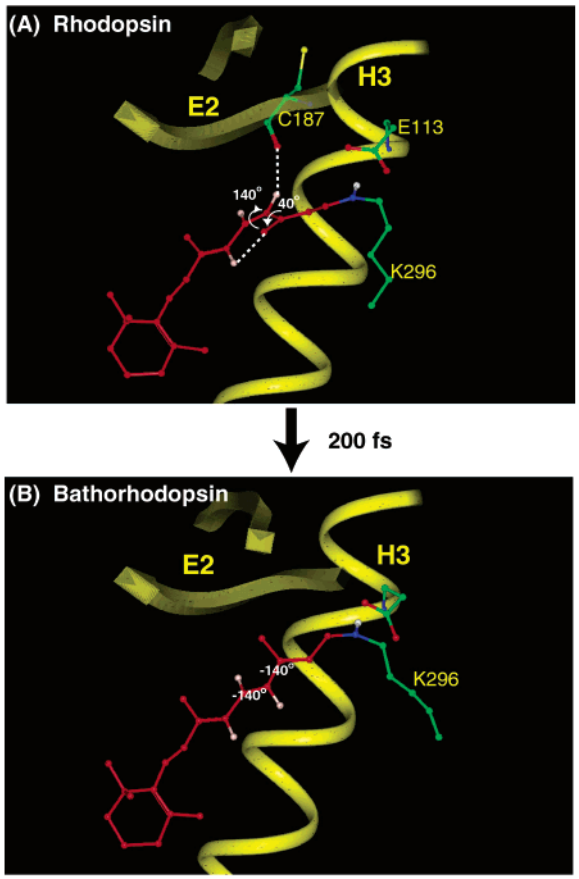

FIGURE 9: (A) Absolute sense and magnitude of the rotations at the C_{11}=C_{12} and C_{12}−C_{13} bonds during the cis−trans isomerization in rhodopsin. Steric repulsion between C_{12}H and Cys187 and between the 13-methyl group and C_{10}H are indicated by the dashed lines. The C_{11}=C_{12} bond rotates in a clockwise sense (view from lysine 296) to carry C_{12}H away from Cys187 and the 13-methyl group away from C_{10}H to release the steric repulsions. (B) Proposed conformation and configuration of the twisted ethylenic chain in the Batho chromophore after photoisomerization.

strated that the HOOP intensities and decoupling decrease as Batho decays through BSI and Lumirhodopsin to Meta I, suggesting a gradual relaxation of the distortion along the photoactivation pathway (*16*, *17*). The transduction of this torsional energy presumably drives the movements of E2 through the steric interactions at the 9- and 13-methyl groups, as well as the movement of H3 through the electrostatic interaction of Glu113 (on H3) with the PSB. The induced E2 and H3 movements coordinated by the functionally important disulfide bond (*63*) may further couple to the hydrogen-bond network in the binding pocking that conducts the counterion switch process (*19*).

Torsional strain along the ethylenic chain has been previously proposed as a mechanism for energy storage in the Batho chromophore (*12*−*14*). Since the first crystal structure of rhodopsin was published in 2000 (*32*), a number of molecular dynamics calculations have been performed to model the Batho structure (*64*−*66*). Although these studies proposed various reaction pathways for the primary photoevent, they consistently produced a highly distorted Batho chromophore. Ishiguro et al. (*66*) described the primary photoevent as the Hula-twist (*58*) isomerization of the C_{11}=C_{12}−C_{13} portion of the molecule followed by an induced rotation of the Schiff base end of the chromophore. Their final Batho chromophore structure has a −148° twist at the C_{11}=C_{12} and a −172° twist at the C_{12}−C_{13} bond. Their predicted same-sense dihedral twists at the C_{11}=C_{12} and C_{12}−C_{13} bonds are consistent with our Batho structure. Rohrig et al. (*65*) used molecular dynamics simulations to monitor the relaxation of the chromophore in the binding pocket after forcing the C_{11}=C_{12} bond to undergo cis−trans isomerization. They found that the early photoproduct is twisted in the same sense at the C_{11}=C_{12} and C_{12}−C_{13} bonds by −161° and −171°, respectively. Interestingly, their photoproduct is highly twisted only when there is a salt bridge at the PSB. This result supports our three-point anchoring model, where the PSB−Glu113 salt-bridge interaction plays an essential role in twisting the ethylenic chain.

CONCLUSIONS

We have tested and disproved the hypothesis that Glu181 is the perturbation that causes the unique decoupled HOOP modes in Batho. Theoretical calculations are then used to support the idea that the C_{11}=C_{12} HOOP decoupling is caused by torsional distortion about *both* the C_{11}=C_{12} and C_{12}−C_{13} bonds in the same sense with a magnitude of ∼40°. On the basis of the crystal structure of bovine rhodopsin, we propose that the absolute dihedral angles at C_{11}=C_{12} and C_{12}−C_{13} in the Batho chromophore are both negative with values of about −140°. Analysis of the Batho HOOP modes and of the protein sequence suggests that the distortion occurs because the chromophore is constrained by protein−chromophore interactions at three points: (1) the PSB is anchored through electrostatic interaction with the Glu113 counterion; (2) the 9-methyl group is constrained through steric interactions with Thr118, Gly188, and Ile189; and (3) the 13-methyl group is constrained through steric interaction with Ala117. Because distorted chromophores with enhanced HOOP modes are commonly observed in the primary photoproducts of photoactive proteins such as bacteriorhodopsin (*2*, *3*), halorhodopsin (*4*), photoactive yellow protein (*5*), and phytochrome (*6*, *7*), each of which involves rapid photoisomerzation about an ethylenic bond, we anticipate that the protein-mediated distortion about the conjugated ethylenic groups that we have uncovered may be a general mechanism for energizing protein conformational changes in light-driven proteins.

ACKNOWLEDGMENT

We thank Douhai Pan for valuable discussions and Sangwoon Yoon for assistance with the calculations.

REFERENCES

1. Mathies, R. A., and Lugtenburg, J. (2000) The primary photoreaction of rhodopsin, in *Molecular Mechanisms in Visual Transduction* (Stavenga, D. G., DeGrip, W. J., and Pugh, E. N. J., Eds.) pp 55−90, Elsevier Science B. V., Amsterdam, The Netherlands.
2. Kochendoerfer, G. G., and Mathies, R. A. (1995) Ultrafast spectroscopy of rhodopsins−Photochemistry at its best! *Isr. J. Chem. 35*, 211−226.
3. Haupts, U., Tittor, J., and Oesterhelt, D. (1999) Closing in on bacteriorhodopsin: Progress in understanding the molecule, *Annu. Rev. Biophys. Biomol. Struct. 28*, 367−399.
4. Dioumaev, A. K., and Braiman, M. S. (1997) Nano- and microsecond time-resolved FTIR spectroscopy of the halorhodopsin photocycle, *Photochem. Photobio. 66*, 755−763.
5. Hellingwerf, K. J., Hendriks, J., and Gensch, T. (2003) Photoactive yellow protein, a new type of photoreceptor protein: Will this

"yellow lab" bring us where we want to go? *J. Phys. Chem. A 107*, 1082−1094.
6. Kneip, C., Hildebrandt, P., Schlamann, W., Braslavsky, S. E., Mark, F., and Schaffner, K. (1999) Protonation state and structural changes of the tetrapyrrole chromophore during the P-r → P-fr phototransformation of phytochrome: A resonance Raman spectroscopic study, *Biochemistry 38*, 15185−15192.
7. Williams, R. E., and Braslavsky, S. E. (2001) in *Comprehensive Series in Photosciences* (Hader, D.-P., and Bert, M., Eds.) pp 15−50, Elsevier, Amsterdam, The Netherlands.
8. Schoenlein, R. W., Peteanu, L. A., Mathies, R. A., and Shank, C. V. (1991) The 1st step in vision-femtosecond isomerization of rhodopsin, *Science 254*, 412−415.
9. Peteanu, L. A., Schoenlein, R. W., Wang, Q., Mathies, R. A., and Shank, C. V. (1993) The 1st step in vision occurs in femtoseconds−Complete blue and red spectral studies, *Proc. Natl. Acad. Sci. U.S.A. 90*, 11762−11766.
10. Kim, J. E., Tauber, M. J., and Mathies, R. A. (2001) Wavelength-dependent cis−trans isomerization in vision, *Biochemistry 40*, 13774−13778.
11. DeLange, F., Bovee-Geurts, P. H. M., VanOostrum, J., Portier, M. D., Verdegem, P. J. E., Lugtenburg, J., and DeGrip, W. J. (1998) An additional methyl group at the 10-position of retinal dramatically slows down the kinetics of the rhodopsin photocascade, *Biochemistry 37*, 1411−1420.
12. Cooper, A. (1979) Energy uptake in the 1st step of visual excitation. *Nature 282*, 531.
13. Tallent, J. R., Hyde, E. W., Findsen, L. A., Fox, G. C., and Birge, R. R. (1992) Molecular-dynamics of the primary photochemical event in rhodopsin, *J. Am. Chem. Soc. 114*, 1581−1592.
14. Schick, G. A., Cooper, T. M., Holloway, R. A., Murray, L. P., and Birge, R. R. (1987) Energy-storage in the primary photochemical events of rhodopsin and isorhodopsin, *Biochemistry 26*, 2556−2562.
15. Kim, J. E., Pan, D. H., and Mathies, R. A. (2003) Picosecond dynamics of G-protein coupled receptor activation in rhodopsin from time-resolved UV resonance Raman spectroscopy, *Biochemistry 42*, 5169−5175.
16. Pan, D., Ganim, Z., Kim, J. E., Verhoeven, M. A., Lugtenberg, J., and Mathies, R. A. (2002) Time-resolved resonance Raman analysis of chromophore structural changes in the formation and decay of rhodopsin's BSI, *J. Am. Chem. Soc. 124*, 4857−4864.
17. Pan, D., and Mathies, R. A. (2001) Chromophore structure in lumirhdopsin and metarhodopsin I by time-resolved resonance Raman microchip spectroscopy, *Biochemistry 40*, 7929−7936.
18. Siebert, F. (1995) Application of FTIR to the investigation of dark structures and photoreactions of visual pigments, *Isr. J. Chem. 35*, 309−323.
19. Yan, E. C. Y., Kazmi, M. A., Ganim, Z., Hou, J. M., Pan, D. H., Chang, B. S. W., Sakmar, T. P., and Mathies, R. A. (2003) Retinal counterion switch in the photoactivation of the G protein-coupled receptor rhodopsin, *Proc. Natl. Acad. Sci. U.S.A. 100*, 9262−9267.
20. Hofmann, K. P., Jager, S., and Ernst, O. P. (1995) Structure and function of activated rhodopsin, *Isr. J. Chem. 35*, 339−355.
21. Fung, B. K. K., and Stryer, L. (1980) Photolyzed rhodopsin catalyzes the exchange of GTP for bound GDP in retinal rod outer segments, *Proc. Natl. Acad. Sci. U.S.A. 77*, 2500−2504.
22. Oseroff, A. R., and Callender, R. H. (1974) Resonance Raman spectroscopy of rhodopsin in retinal disk membranes, *Biochemistry 13*, 4243−4248.
23. Peters, K., Applebury, M. L., and Rentzepis, P. M. (1977) Primary photochemical event in vision-proton translocation, *Proc. Natl. Acad. Sci. U.S.A. 74*, 3119−3123.
24. Fransen, M. R., Luyten, W. C. M. M., van Thuijl, J., Lugtenburg, J., Jansen, P. A. A., Vanbreugel, P. J. G. M., and Daemen, F. J. M. (1976) Structure of chromophoric group in bathorhodopsin, *Nature 260*, 726−727.
25. Eyring, G., and Mathies, R. A. (1979) Resonance Raman studies of bathorhodopsin−Evidence for a protonated Schiff-base linkage, *Proc. Natl. Acad. Sci. U.S.A. 76*, 33−37.
26. Eyring, G., Curry, B., Mathies, R., Fransen, R., Palings, I., and Lugtenburg, J. (1980) Interpretation of the resonance Raman-spectrum of bathorhodopsin based on visual pigment analogs, *Biochemistry 19*, 2410−2418.
27. Eyring, G., Curry, B., Broek, A., Lugtenburg, J., and Mathies, R. (1982) Assignment and interpretation of hydrogen out-of-plane vibrations in the resonance Raman-spectra of rhodopsin and bathorhodopsin, *Biochemistry 21*, 384−393.
28. Palings, I., Van den Berg, E. M. M., Lugtenburg, J., and Mathies, R. A. (1989) Complete assignment of the hydrogen out-of-plane wagging vibrations of bathorhodopsin: Chromophore structure and energy storage in the primary photoproduct of vision, *Biochemistry 28*, 1498−1507.
29. Han, M., and Smith, S. O. (1995) NMR constraints on the location of the retinal chromophore in rhodopsin and bathorhodopsin, *Biochemistry 34*, 1425−1432.
30. Smith, S. O., Courtin, J., DeGroot, H., Gebhard, R., and Lugtenburg, J. (1991) C-13 magic-angle spinning NMR-studies of bathorhodopsin, the primary photoproduct of rhodopsin, *Biochemistry 30*, 7409−7415.
31. Warshel, A., and Barboy, N. (1982) Energy-storage and reaction pathways in the 1st step of the vision process, *J. Am. Chem. Soc. 104*, 1469−1476.
32. Van Hooser, J. P., Aleman, T. S., He, Y. G., Cideciyan, A. V., Kuksa, V., Pittler, S. J., Stone, E. M., Jacobson, S. G., and Palczewski, K. (2000) Rapid restoration of visual pigment and function with oral retinoid in a mouse model of childhood blindness, *Proc. Natl. Acad. Sci. U.S.A. 97*, 8623−8628.
33. Okada, T., Fujiyoshi, Y., Silow, M., Navarro, J., Landau, E. M., and Shichida, Y. (2002) Functional role of internal water molecules in rhodopsin revealed by X-ray crystallography, *Proc. Natl. Acad. Sci. U.S.A. 99*, 5982−5987.
34. Teller, D. C., Okada, T., Behnke, C. A., Palczewski, K., and Stenkamp, R. E. (2001) Advances in determination of a high-resolution three-dimensional structure of rhodopsin, a model of G-protein-coupled receptors (GPCRs), *Biochemistry 40*, 7761−7772.
35. Okada, T., Ernst, O. P., Palczewski, K., and Hofmann, K. P. (2001) Activation of rhodopsin: New insights from structural and biochemical studies, *Trends Biochem. Sci. 26*, 318−324.
36. Yan, E. C. Y., Kazmi, M. A., De, S., Chang, B. S. W., Seibert, C., Marin, E. P., Mathies, R. A., and Sakmar, T. P. (2002) Function of extracellular loop 2 in rhodopsin: Glutamic acid 181 modulates stability and absorption wavelength of metarhodopsin II, *Biochemistry 41*, 3620−3627.
37. Min, K. C., Zvyaga, T. A., Cypess, A. M., and Sakmar, T. P. (1993) Characterization of mutant rhodopsins responsible for autosomal-dominant retinitis-pigmentosa-mutations on the cytoplasmic surface affect tranducin activation, *J. Biol. Chem. 268*, 9400−9404.
38. Han, M., Lin, S. W., Minkova, M., Smith, S. O., and Sakmar, T. P. (1996) Functional interaction of transmembrane helices 3 and 6 in rhodopsin: Replacement of phenylalanine 261 by alanine causes reversion of phenotype of a glycine 121 replacement mutant, *J. Biol. Chem. 271*, 32337−32342.
39. Palings, I., Pardoen, J. A., Vandenberg, E., Winkel, C., Lugtenburg, J., and Mathies, R. A. (1987) Assignment of fingerprint vibrations in the resonance Raman-spectra of rhodopsin, isorhodopsin, and bathorhodopsin−Implications for chromophore structure and environment, *Biochemistry 26*, 2544−2556.
40. Frisch, M. J., Trucks, G. W., Schlegel, H. B., Scuseria, G. E., Robb, M. A., Cheeseman, J. R., Zakrzewski, V. G., Montgomery, J. A., Jr., Stratmann, R. E., Burant, J. C., Dapprich, S., Millam, J. M., Daniels, A. D., Kudin, K. N., Strain, M. C., Farkas, O., Tomasi, J., Barone, V., Cossi, M., Cammi, R., Mennucci, B., Pomelli, C., Adamo, C., Clifford, S., Ochterski, J., Petersson, G. A., Ayala, P. Y., Cui, Q., Morokuma, K., Rega, N., Salvador, P., Dannenberg, J. J., Malick, D. K., Rabuck, A. D., Raghavachari, K., Foresman, J. B., Cioslowski, J., Ortiz, J. V., Baboul, A. G., Stefanov, B. B., Liu, G., Liashenko, A., Piskorz, P., Komaromi, I., Gomperts, R., Martin, R. L., Fox, D. J., Keith, T., Al-Laham, M. A., Peng, C. Y., Nanayakkara, A., Challacombe, M., Gill, P. M. W., Johnson, B., Chen, W., Wong, M. W., Andres, J. L., Gonzalez, C., Head-Gordon, M., Replogle, E. S., and Pople, J. A. (2001) Gaussian, Inc., Pittsburgh, PA.
41. Becke, A. D. (1993) Density-functional thermochemistry. III. The role of exact exchange, *J. Chem. Phys. 98*, 5648−5652.
42. Lee, H. M., Kim, J., Kim, C., and Kim, K. S. (2002) Ab Initio study of the isomerization of retinal chromophore and its derivatives, *J. Chem. Phys. 116*, 6549−6559.
43. Tasumi, M., Sakamoto, A., Hieda, T., and Torii, H. (2002) Use of group theory for band assignment and structure correlation, in *Handbook of Vibrational Spectroscopy* (Chalmers, J. M., and Griffin, P. R., Eds.) Vol. 3, pp 1983−1991, John Wiley and Sons, Chichester, U.K.
44. Oakes, R. E., Spence, S. J., and Bell, S. E. J. (2003) Resonance Raman and DFT studies of tera-tetra-butyl Porphine: Assignment

of strongly enhanced distortion modes in a ruffled porphyrin, *J. Phys. Chem. A 107*, 2964−2973.
45. Gervasio, F. L., Cardini, G., Salvi, P. R., and Schettino, V. (1998) Low-frequency vibrations of all-*trans*-retinal: Far-infrared and Raman spectra and density functional calculations, *J. Phys. Chem. A 102*, 2131−2136.
46. Hashimito, H., Hattori, K., Okada, Y., Yoda, T., and Matsushima, R. (1998) Molecular and crystal structures of 2-(all-*trans*-retinylidene)-indan-1,3-dione, *Jpn. J. Appl. Phys. 37*, 4609−4615.
47. Froese, R. D. J., Komaromi, I., Byun, K. S., and Morokuma, K. (1997) Theoretical studies of protonated and non-protonated Schiff bases of retinal: Ground-state structures and energies of the all-trans, 13-cis, 11-cis, 9-cis, 6,7-cis, and 6-s-cis isomers, *Chem. Phys. Lett. 272*, 335−340.
48. Curry, B., Broek, A., Lugtenburg, J., and Mathies, R. (1982) Vibrational analysis of all-*trans*-retinal, *J. Am. Chem. Soc. 104*, 5274−5286.
49. Lin, S. W., Groesbeek, M., van der Hoef, I., Verdegem, P., Lugtenburg, J., and Mathies, R. A. (1998) Vibrational assignment of torsional normal modes of rhodopsin: Probing excited-state isomerization dynamics along the reactive C_{11}═C_{12} torsion coordinate, *J. Phys. Chem. B 102*, 2787−2806.
50. Schaftenaar, G., and Noordik, J. H. (2000) Molden: A pre- and post-processing program for molecular and electronic structures, *J. Comput.-Aided Mol. Des. 14*, 123−134.
51. Curry, B., Palings, I., Broek, A. D., Pardoen, J. A., Lugtenburg, J., and Mathies, R. A. (1985) in *Advances in Infrared and Raman Spectroscopy* (Clark, J. H., and Hester, R. E., Eds.) pp 115, Wiley Heyden, New York.
52. Baasov, T., Friedman, N., and Sheves, M. (1987) Factors affecting the C═N stretching in protonated retinal Schiff base: A model study for bacteriorhodspsin and visual pigments, *Biochemistry 26*, 3210−3217.
53. Lin, S. W., Sakmar, T. P., Franke, R. R., Khorana, H. G., and Mathies, R. A. (1992) Resonance Raman microprobe spectroscopy of rhodopsin mutants: Effect of substitutions in the third transmembrane helix, *Biochemistry 31*, 5105−5111.
54. Barry, B., and Mathies, R. A. (1987) Raman microscope studies on the primary photochemistry of vertebrate visual pigments with absorption maxima from 430 to 502 nm, *Biochemistry 26*, 59−64.
55. Lin, S. W., Imamoto, Y., Fukada, Y., Shichida, Y., Yoshizawa, T., and Mathies, R. A. (1994) What makes red visual pigments red—A resonance Raman microprobe study of retinal chromophore structure in iodopsin, *Biochemistry 33*, 2151−2160.
56. Deng, H., Manor, D., Weng, G., Rath, P., Koutalos, Y., Ebrey, T., Gebhard, R., Lugtenburg, J., Tsuda, M., and Callender, R. H. (1991) Resonance Raman studies of the HOOP modes in octopus bathorhodopsin with deuterium-labeled retinal chromophores, *Biochemistry 30*, 4495−4502.
57. Nagata, T., Oura, T., Terakita, A., Kandori, H., and Shichida, Y. (2002) Isomer-specific interaction of the retinal chromophore with threonine-118 in rhodopsin, *J. Phys. Chem. A 106*, 1969−1975.
58. Liu, R. S. H., and Colmenares, L. U. (2003) The molecular basis for the high photosensitivity of rhodopsin, *Proc. Natl. Acad. Sci. U.S.A. 100*, 14639−14644.
59. Klyne, W., and Prelog, V. (1960) Description of steric relationships across single bonds, *Experientia 16*, 521−523.
60. Wilson, E. B., Jr., Decius, J. C., and Cross, P. C. (1980) *Molecular Vibrations*, Dover Publications, Inc., New York.
61. Gerwert, K., and Siebert, F. (1986) Evidence for ligh-induced 13-cis, 14-s-cis isomerization in bacteriorhodopsin obtained by FTIR difference spectroscopy using isotopically labeled retinals, *EMBO J. 5*, 805−811.
62. Brudler, R., Rammelsberg, R., Woo, T. T., Getzoff, E. D., and Gerwert, K. (2001) Structure of the I-1 early intermediate of photoactive yellow protein by FTIR spectroscopy, *Nat. Struct. Biol. 8*, 265−270.
63. Farrens, D. L., Altenbach, C., Yang, K., Hubbell, W. L., and Khorana, H. G. (1996) Requirement of rigid-body motion of transmembrane helices for light activation of rhodopsin, *Science 274*, 768−770.
64. Schreiber, M., and Buss, V. (2003) Origin of the bathochromic shift in the early photointermediates of the rhodopsin visual cycle: A CASSCF/CASPT2 study, *Int. J. Quantum Chem. 95*, 882−889.
65. Rohrig, U. F., Guidoni, L., and Rothlisberger, U. (2002) Early steps of the intramolecular signal transduction in rhodopsin explored by molecular dynamics simulations, *Biochemistry 41*, 10799−10809.
66. Ishiguro, M., Hirano, T., and Oyama, Y. (2003) Modelling of photointermediates suggests a mechanism of the flip of the β-ionone moiety of the retinylidene chromophore in the rhodopsin photocascade, *ChemBioChem 4*, 228−231.

BI0400148